Materials Research. 2014; 17(2): 405-411
DOI: http://dx.doi.org/10.1590/S1516-14392013005000192

Effects of Precursor Concentration and Reaction Time on Sonochemically Synthesized ZnO Nanoparticles

Chat Pholnak[a], Chitnarong Sirisathitkul[a], Sumetha Suwanboon[b], David James Harding[a]*

[a]*Molecular Technology Research Unit, School of Science, Walailak University – WU, 80160, Nakhon Si Thammarat, Thailand*
[b]*Department of Materials Science and Technology, Faculty of Science, Prince of Songkla University – PSU, 90112, Hat Yai, Songkhla, Thailand*

Received: April 20, 2013; Revised: October 25, 2013

The sonochemical reaction between $Zn(NO_3)_2$ and hexamethylenetetramine (HMT) resulted in different products depending on amounts of Zn(II) cations in the aqueous solution. Crystalline phase pure ZnO nanoparticles were obtained by using 0.05 M $Zn(NO_3)_2$-HMT. This single phase was formed by low power sonication for 20 min in an ultrasonic bath at ambient conditions and its morphology did not change for the next 60 min. Higher concentrations of precursors (0.1 and 0.5 M) led to a mixture of zinc compounds including plate-like $Zn_5(OH)_8(NO_3)_2(H_2O)$. In contrast, a mixed phase $ZnO/Zn_5(OH)_6(CO_3)_2$ and a single phase $Zn_5(OH)_6(CO_3)_2$ were formed when the precursor concentrations were decreased to 0.01 and 0.005 M, respectively. The resulting infrared absorption and ultraviolet/visible emission were dependent on the phases and defects in these zinc compounds.

Keywords: *ZnO, FTIR, photoluminescence, sonochemistry*

1. Introduction

Research and development in sonochemically synthesized zinc oxide (ZnO) has led to significant theoretical and technological progresses since 2004[1]. Theoretical studies suggest that the mechanism of ZnO formation involves acoustic cavitation upon ultrasonic irradiation. Jung et al. proposed the evolution of sonicated ZnO nuclei into spheres (isotropic growth), disks (suppression of 1-D growth), rods (1-D growth) and flower-like ZnO (multiple nanorods growth)[2]. In terms of technological advances, multifunctional ZnO with mechanical, physical, chemical and biological utility can now be synthesized using low-cost sonoreactors. Moreover, many commercial ultrasonic probes and baths are also available. A variety of ZnO morphologies ranging from spheres[2], flower-like[2], cauliflower-like[3], needle-like[4], sword-like[5], octahedra[6], nanosheets[7], hexagonal nanotubes[2,8] to nanorods[1,2,9-11] are obtained by variations in the sonochemical conditions. The morphologies are also dependent on the type of precursors and may result in other zinc compounds. In work by Gusatti et al.[12], a mixed phase material consisting of $Zn_5(OH)_8Cl_2{\cdot}H_2O$ and ZnO was obtained by sonicating $ZnCl_2$ while under similar conditions the use of zinc nitrate hexahydrate ($Zn(NO_3)_2{\cdot}6H_2O$) produced pure ZnO. Our previous work has shown that sonication of highly concentrated $Zn(NO_3)_2{\cdot}6H_2O$ and hexamethylenetetramine (HMT) solutions gives rise to zinc hydroxide nitrate hydrate ($Zn_5(OH)_8(NO_3)_2(H_2O)_2$)[6]. This zinc compound is an intermediate product which transforms into ZnO upon heat treatment. Since the concentration of the precursors clearly plays an important role in dictating the phase and morphology of the products from the sonochemical reaction, its effect and sonication time are investigated in this work.

*e-mail: chitnarong.siri@gmail.com

2. Experimental Procedure

Reagent grade $Zn(NO_3)_2{\cdot}6H_2O$ and HMT powders (≥ 99.0% in purity) were used as precursors without any pretreatment. Aqueous solutions of the two starting materials were mixed under vigorous stirring (600 rpm) and heated to 50 °C. Once the solution turned into a stable viscous white colloid, the stirring was continued for another 10 min. The colloid was then transferred to a commercial ultrasonic bath (Kerry KC3) which, at a maximum electrical power of 75W, supplied a continuous 38 kHz ultrasonic wave under ambient conditions. After sonication, the white precipitate was collected by filtration and thoroughly rinsed with distilled water and ethanol. Finally, the precipitate was dried in an oven at 100 °C in an air atmosphere for 2 h. The effect of concentration was investigated using $Zn(NO_3)_2{\cdot}6H_2O$ and HMT concentrations of 0.005, 0.01, 0.05, 0.1 and 0.5 M while keeping the sonication time constant at 60 min. These samples are referred to as F1-F5 listed in Table 1. To examine the effect of reaction time, four more samples (G1-G4) were prepared from 0.05 M $Zn(NO_3)_2$-HMT using sonication times of 20, 40, 60 and 80 min.

Powder X-ray diffraction (XRD, Philips X' Pert MPD) of the synthesized products were carried out using Cu$K\alpha$ radiation (λ = 1.54056 Å). The morphologies were inspected by scanning electron microscopy (SEM, FEI Quanta 400) operating at 25 kV. The particle size of each nanoparticle was measured using the Image J program. The Fourier transform infrared (FTIR) spectra

were obtained from pellets of the synthesized powder mixed with potassium bromide (KBr) by using a Perkin Elmer Spectrum One spectrophotometer. A milligram of each sample was mixed and crushed with about 0.2 g of dried KBr. The samples were formed into pellets 13 mm in diameter and 0.5 mm in thickness by mould pressing. The FTIR measurements were performed on the pellets placed in a window of IR radiation with measurements recorded between 350-4000 cm^{-1} at a resolution of 4 cm^{-1}. The room temperature photoluminescence (PL) spectrum was measured using a luminescence spectrometer (LS/55, PerkinElmer).

3. Results and Discussion

3.1. *Effect of $Zn(NO_3)_2$-HMT concentrations*

During the reaction, the temperature of the colloid was gradually raised. The heating rate was decreased with the increase in concentration from 0.1675 °C/min (0.005 M) to 0.0578 °C/min (0.5 M). XRD patterns obtained from samples F1-F5 are shown in Figure 1 and the crystalline phases are summarized in Table 1. The concentration of $Zn(NO_3)_2$ and HMT were found to significantly impact the phase and purity of the Zn products. In Figure 1a, sample F1 prepared from the lowest concentration attempted in this study is identified as hydrozincite ($Zn_5(OH)_6(CO_3)_2$) (JCPDS card No. 01-072-1100) whose structure is monoclinic C2/m[13]. The hydrolysis of HMT releases NH_4^+ cations and OH^- anions as shown in Equations 1.1 and 1.2 and the dissolution of $Zn(NO_3)_2{\cdot}6H_2O$ leads to Zn^{2+} cations as indicated in Equation 2. In Equation 3, CO_3^{2-} is created by the reaction of the OH^- anions and CO_2 from the air. The formation of $Zn_5(OH)_6(CO_3)_2$ is then produced by the sonochemical reaction shown in Equation 4.

$$C_6H_{12}N_4 + 6H_2O \rightarrow 4NH_3 + 6HCHO \quad (1.1)$$

$$NH_3 + H_2O \rightarrow NH_4^+ + OH^- \quad (1.2)$$

$$Zn(NO_3)_2 \cdot 6H_2O \rightarrow Zn^{2+}(aq) + 2NO_3^-(aq) \quad (2)$$

$$CO_2 + 2OH^- \rightarrow CO_3^{2-} + H_2O \quad (3)$$

$$5Zn^{2+} + 6OH^- + 2CO_3^{2-} \xrightarrow{)))} Zn_5(CO_3)_2(OH)_6 \quad (4)$$

In the case of 0.01 M $Zn(NO_3)_2$-HMT, the XRD pattern of sample F2 in Figure 1b indicates a mixture of hexagonal wurtzite ZnO with a space group of P63mc (JCPDF card No. 01-079-2205) and $Zn_5(OH)_6(CO_3)_2$. The crystalline ZnO is formed by between a higher concentration of Zn(II) radicals and the hydroxide radicals in the sonochemical reactions according to Equation 5.1 and 5.2.

$$Zn^{2+} + 4OH^- \rightarrow Zn(OH)_4^{2-} \xrightarrow{)))} ZnO + H_2O + 2OH^- \quad (5.1)$$

$$Zn^{2+} + 2OH^- \rightarrow Zn(OH)_2 \xrightarrow{)))} ZnO + H_2O \quad (5.2)$$

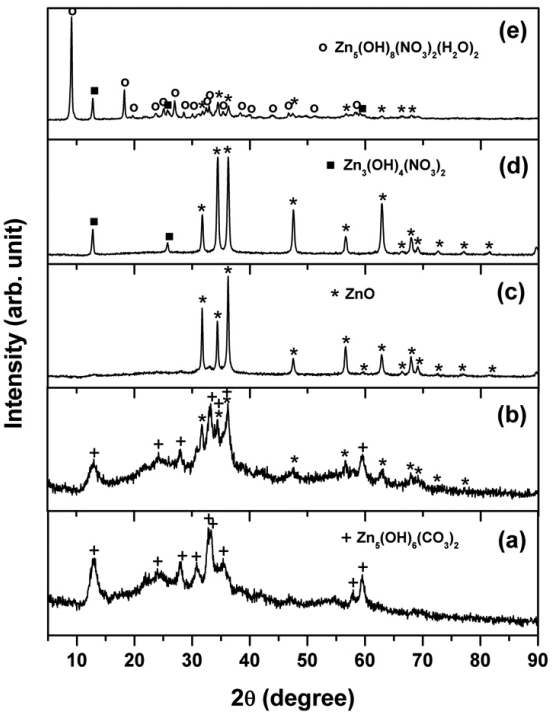

Figure 1. XRD patterns of samples: (a) F1, (b) F2, (c) F3, (d) F4 and (e) F5.

Table 1. Phase and morphology of zinc compounds prepared from sonochemical reactions with varying precursor concentrations (F1-F5) and reaction times (G1-G4).

Sample	Irradiation time (min)	Molar concentration (M)		Crystalline phase	Morphology
		$Zn(NO_3)_2{\cdot}6H_2O$	$C_6H_{12}N_4$		
F1	60	0.005	0.005	$Zn_5(OH)_6(CO_3)_2$	Nanospheroids
F2	60	0.01	0.01	$ZnO/Zn_5(OH)_6(CO_3)_2$	Nanospheroids
F3	60	0.05	0.05	ZnO	Nanospheroids
F4	60	0.1	0.1	$ZnO/Zn_3(OH)_4(NO_3)_2$	Nanospheroids
F5	60	0.5	0.5	$ZnO/Zn_3(OH)_4(NO_3)_2/$ $Zn_5(OH)_8(NO_3)_2(H_2O)_2$	Microplates
G1	20	0.05	0.05	ZnO	Nanospheroids
G2	40	0.05	0.05	ZnO	Nanospheroids
G3	60	0.05	0.05	ZnO	Nanospheroids
G4	80	0.05	0.05	ZnO	Nanospheroids

The peaks of $Zn_5(OH)_6(CO_3)_2$ are understandably lower than those of the single phase $Zn_5(OH)_6(CO_3)_2$ shown in Figure 1a. In both Figures 1a and b, samples F1 and F2 also contain an amorphous phase so lower and broader peaks contribute to a noisy background.

Since the major peak of $Zn_5(OH)_6(CO_3)_2$ at 33° is only just visible in Figure 1c, the XRD pattern of sample F3 (0.05 M $Zn(NO_3)_2$-HMT) exhibits a single crystalline phase of hexagonal wurtzite ZnO. Compared to the XRD patterns in Figures 1a and b, the higher peak intensity and narrower peaks indicate high product crystallinity and result in the smooth pattern obtained due to its higher signal to noise ratio. This result is in good agreement with previous experimental findings using the same concentration in different sonoreactors[6]. The phase purity of this sample indicates that this concentration is recommended for the synthesis of high purity ZnO from $Zn(NO_3)_2$-HMT.

By increasing the $Zn(NO_3)_2$-HMT concentration to 0.1 M, ZnO is still the dominant phase in sample F4 but a second phase identified as monoclinic zinc hydroxide nitrate

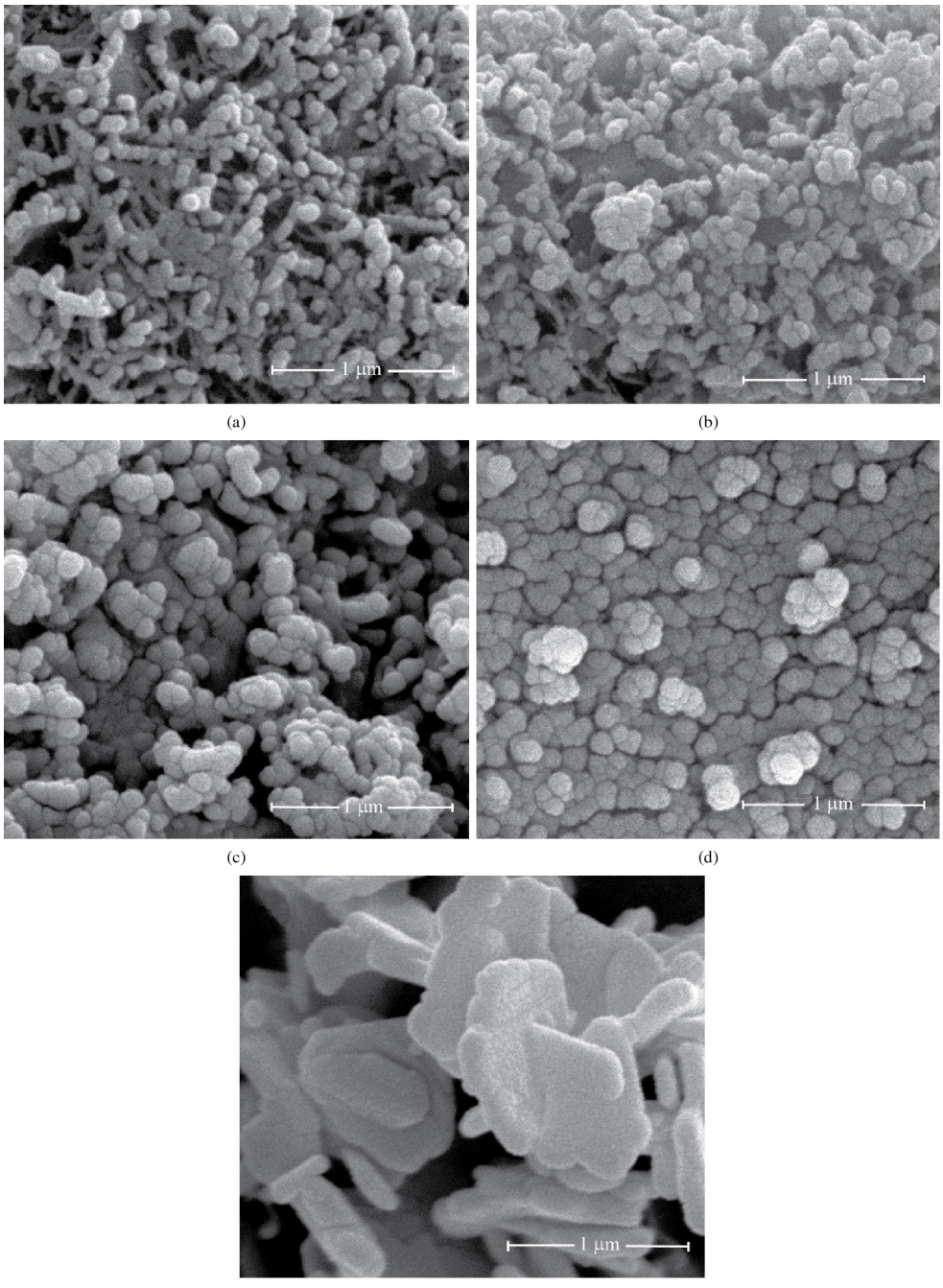

Figure 2. SEM micrographs of samples: (a) F1, (b) F2, (c) F3, (d) F4 and (e) F5.

($Zn_3(OH)_4(NO_3)_2$) with a space group C21/c is introduced (JCPDF card No.00-052-0627). As shown in Figure 1d, the diffraction peaks at 12.8° and 25.7° correspond to the (100) and (200) planes. Increasing the concentration of the precursors further to 0.5 M (sample F5) leads to another phase, making a total of three phases which may be indexed in the XRD pattern in Figure 1e. In addition to the characteristic ZnO and $Zn_3(OH)_4(NO_3)_2$ peaks, major peaks for zinc hydroxide nitrate hydrate ($Zn_5(OH)_8(NO_3)_2(H_2O)_2$) are found at 9.12° and 18.3° due to the (200) and (401) diffraction planes. $Zn_5(OH)_8(NO_3)_2(H_2O)_2$ has a monoclinic structure with a space group C2/m and tends to be the dominant product in the case of highly concentrated $Zn(NO_3)_2$[6]. The formations of $Zn_3(OH)_4(NO_3)_2$ and $Zn_5(OH)_8(NO_3)_2(H_2O)_2$ in sample F5 are respectively described by the sonochemical reactions in Equations 6 and 7.

$$3Zn^{2+} + 4OH^- + 2NO_3^- \xrightarrow{)))} Zn_3(OH)_4(NO_3)_2 \quad (6)$$

$$5Zn^{2+} + 8OH^- + 2NO_3^- + 2H_2O \xrightarrow{)))} Zn_5(OH)_8(NO_3)_2(H_2O)_2 \quad (7)$$

The effect of the precursor concentration on the morphology of products is revealed by SEM images in Figure 2 and summarized in Table 1. By comparing single phase compounds in Figure 2a and Figure 2c, $Zn_5(OH)_6(CO_3)_2$ nanoparticles synthesized from 0.005 M $Zn(NO_3)_2$-HMT (average diameter 87.8 ± 14.0 nm) are smaller than ZnO synthesized from 0.05 M $Zn(NO_3)_2$-HMT (average diameter 109.0 ± 20.5 nm). With the sizes of single phase $Zn_5(OH)_6(CO_3)_2$ in the range of 60-128 nm and ZnO in the range of 80-146 nm, it follows that Figure 2b reveals a mixed phase of ZnO and $Zn_5(OH)_6(CO_3)_2$ spheroids of comparable diameter ranging from 48 to 108 nm with an average value of 81.3 ± 14.7 nm. ZnO and $Zn_3(OH)_4(NO_3)_2$ particles in Figure 2d have a larger average diameter of 141.0 ± 24.9 nm. By contrast, the morphology of mixed phases of ZnO/$Zn_3(OH)_4(NO_3)_2$/$Zn_5(OH)_8(NO_3)_2(H_2O)_2$ in Figure 2e is best described as a microsheet with a size between 0.28 and 1.08 μm. This morphology is identical to a previous observation in $Zn_5(OH)_8(NO_3)_2(H_2O)_2$[6].

FTIR spectra of samples F1-F4 are compared in Figure 3. Predictably, the characteristic band of wurtzite ZnO[2,14-16] in the range of 400-500 cm^{-1} is strongest in the case of single phase ZnO (sample F3) and weakest in the case of $Zn_5(OH)_6(CO_3)_2$ (sample F1). Other marked absorption bands in sample F3 correspond to O-H bending and stretching[17,18]. In the same range of vibrations by residual NO_3^- ions[16], the carbonate stretches in samples F1 and F2 are observed at 1540 and 1480 cm^{-1} and similar to the previous report on sol-gel synthesis of hydrozincite[19]. The peaks at 1052 and 830 cm^{-1} are assigned to the ν_1 and ν_2 stretches of carbonate and are consistent with the carbonates

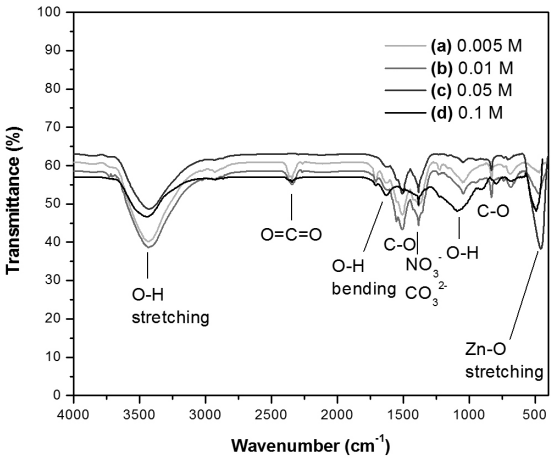

Figure 3. FITR spectra of samples: (a) F1, (b) F2, (c) F3 and (d) F4.

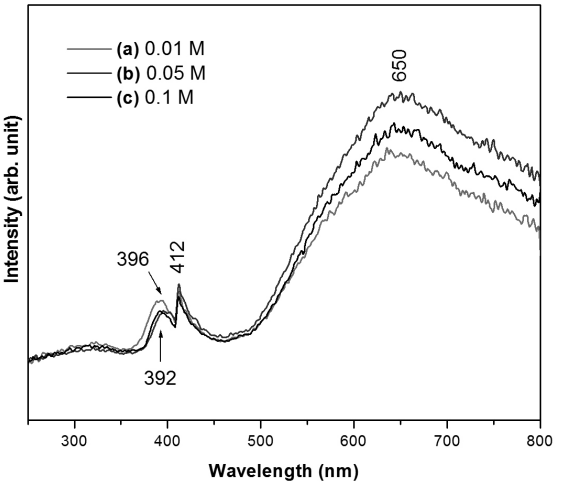

Figure 4. PL spectra of samples: (a) F2, (b) F3 and (c) F4.

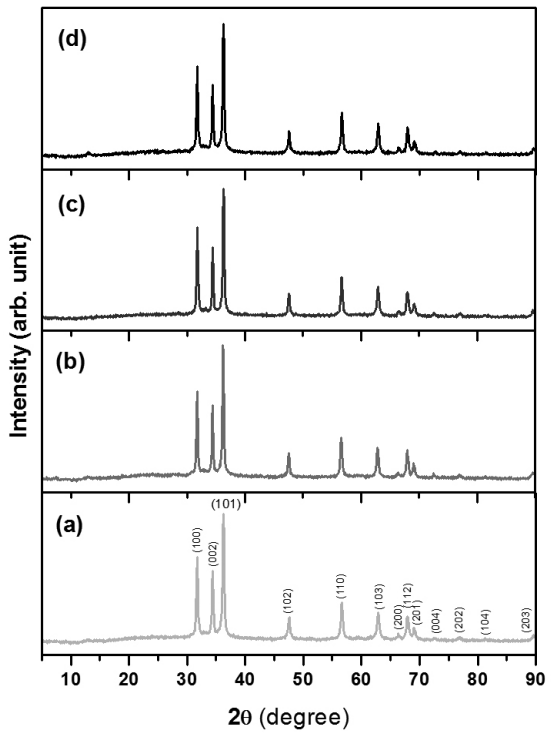

Figure 5. XRD patterns of samples: (a) G1, (b) G2, (c) G3 and (d) G4.

being bound to an octahedral and tetrahedral zinc centre as expected in the hydrozincite structure[20]. In addition, the band centered at 2345 cm^{-1} is present exclusively in samples with $Zn_5(OH)_6(CO_3)_2$ (samples F1 and F2) and is attributed to the absorption of atmospheric CO_2 on the metallic cation[21]. Interestingly, almost identical absorptions due to CO_2 are found in hydrozincite in the literature[19]. ZnO can be prepared from either $Zn_5(OH)_6(CO_3)_2$ [19,22] or $Zn_5(OH)_8(NO_3)_2(H_2O)_2$ [6] by pyrolysis. However, the aim of this research is to sonochemically synthesize ZnO powders of controlled structure and morphology in a single step in order to reduce the cost of production when this is used in the industry. Therefore, the heat treatment was not attempted in this instance.

In Figure 4, all samples exhibit UV emission peaks at 396 nm in their PL spectra corresponding to the near band-edge recombination of excitons in ZnO[1,23-26]. Two peaks at both ends of the visible region from interstitial atoms and vacancies[25] are also observed. The narrow violet emission peak at 412 nm is due to the transition between a shallow defect level and the valence band. The broad red emission peak centered around 650 nm is related to nanostructured ZnO with different morphologies and deep defect levels well below the conduction band. The much higher intensity of this visible peak compared to that of the UV absorption is an indication of a high density of defects in the crystals of ZnO/$Zn_3(OH)_4(NO_3)_2$. The inclusion of $Zn_5(OH)_6(CO_3)_2$ in sample F2 clearly shifts the emission peaks to a lower wavelength.

3.2. *Effect of sonication time*

Since 0.05 M $Zn(NO_3)_2$-HMT in aqueous solutions gives rise to single phase ZnO, this concentration was selected for the study of reaction time. XRD spectra and SEM images of samples G1-G4 sonicated for 20-80 min are shown in Figures 5 and 6 and the results are summarized in Table 1. All samples possess the ZnO wurtzite structure. Without any other impurity peaks, characteristic ZnO peaks are clearly observed at 36.2°, 31.7°, 34.3°, 47.5°, 56.5°, 59.6°, 62.8°, 66.3°, 67.8° and 69.0°, corresponding to the (101), (100), (002), (102), (110), (103), (200), (112), (201) and (004) planes, respectively. The XRD peak width shows little variation with the sonication time from 20 to 80 min. The crystallite size is calculated from the Scherrer formula as 34-43 nm which are comparable to the other works[22] but the crystallites tend to agglomerate as the sonication time is extended as shown by the SEM studies (Figure 6). Spheroidal nanoparticles are observed irrespective of sonication time. Thus, the phase and morphology formed during the initial 20 min of the sonochemical reaction do not change in the next 60 min. The short sonication time of 20 min is therefore sufficient for the synthesis of ZnO

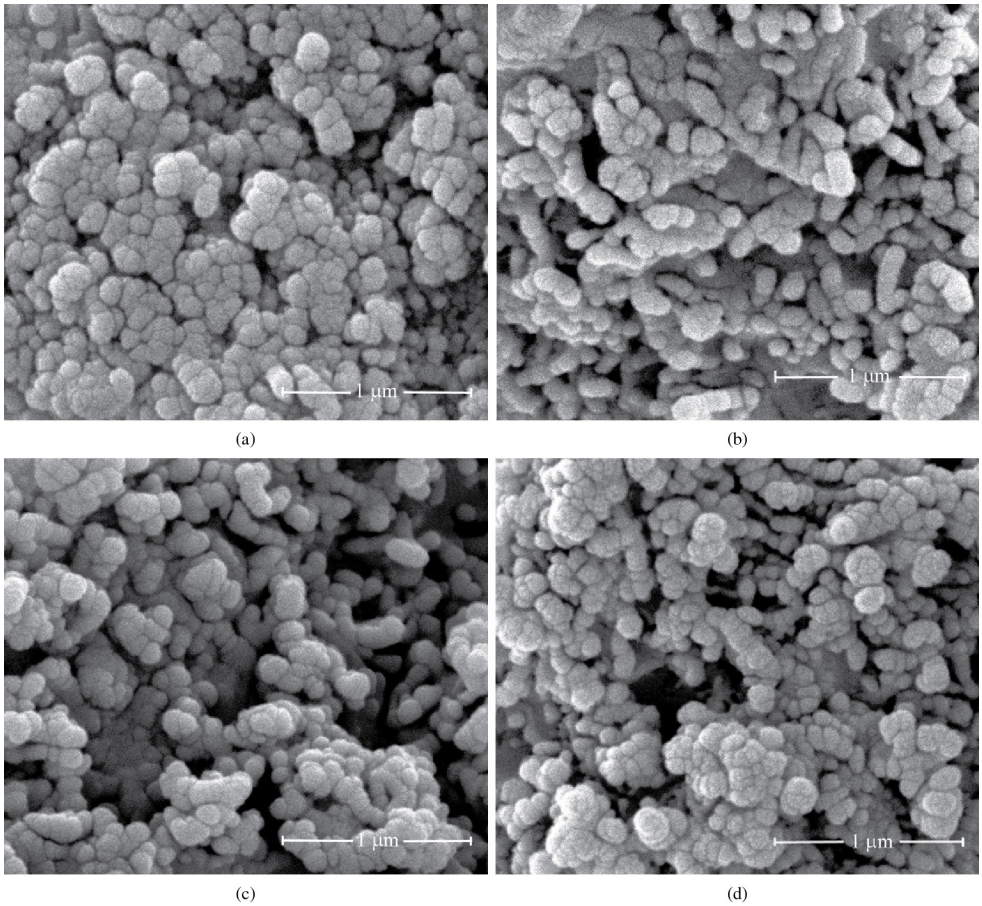

Figure 6. SEM micrographs of samples: (a) G1, (b) G2, (c) G3 and (d) G4.

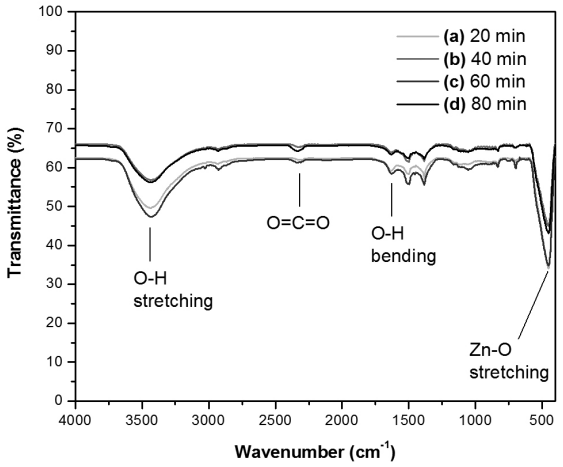

Figure 7. FTIR spectra of samples: (a) G1, (b) G2, (c) G3 and (d) G4.

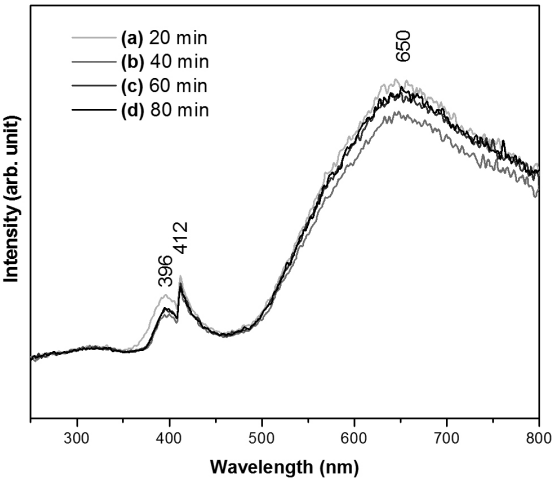

Figure 8. PL spectra of samples: (a) G1, (b) G2, (c) G3 and (d) G4.

nanoparticles in this ultrasonic bath much shorter than that currently employed for commercial synthesis of ZnO.

Figures 7 and 8 do not indicate a large difference in IR absorption and UV-visible emission among samples G1-G4. Only ZnO and O-H stretching bands are pronounced in the FTIR spectra indicating the homogeneous ZnO products. UV, violet and red emission peaks resemble those previously observed in sample F3 with single phase ZnO. All these peaks occur at an identical position for samples G1-G4 with varying sonication times. These optical properties confirm the XRD and SEM results that the variation in sonication time from 20 to 80 min does not lead to significant changes in phase and morphology in the ZnO products. Nevertheless, the density of defects, compared by the ratio of UV to visible peak intensities[22,27], is varied.

4. Conclusions

ZnO nanoparticles were grown after 20 min of sonication from a 0.05 M $Zn(NO_3)_2$-HMT solution. Changing the concentration of the precursors resulted in formation of other zinc compounds. Thus, a mixed phase of plate-like $Zn_5(OH)_8(NO_3)_2(H_2O)_2$ and ZnO formed when the concentration was 0.5 M. On the other hand, lower concentrations of 0.01 M gave rise to a $ZnO/Zn_5(OH)_6(CO_3)_2$ mixture while $Zn_5(OH)_6(CO_3)_2$ was the only phase found at 0.005 M. The phases and crystalline defects of these zinc compounds were confirmed by FTIR and PL spectra. Overall, the short reaction time and consistent morphology at 0.05 M suggest this is a promising technique for preparation of ZnO nanospheroids.

Acknowledgements

This work is funded by Walailak University (Grant no. WU55302). The authors would like to thank the Scientific Equipment Center of Prince of Songkla University and Walailak University for access to characterization facilities.

References

1. Hu XL, Zhu YJ and Wang SW. Sonochemical and microwave-assisted synthesis of linked single-crystalline ZnO rods. *Materials Chemistry and Physics*. 2004; 88:421-426. http://dx.doi.org/10.1016/j.matchemphys.2004.08.010
2. Jung SH, Oh E, Lee KH, Yang Y, Park CG, Park WJ et al. Sonochemical preparation of shape-selective ZnO nanostructures. *Crystal Growth and Design*. 2008; 8:265-269. http://dx.doi.org/10.1021/cg070296l
3. Mazloumi M, Zanganeh S, Kajbafvala A, Ghariniyat P, Taghavi S, Lak A et al. Ultrasonic induced photoluminescence decay in sonochemically obtained cauliflower-like ZnO nanostructures with surface 1D nanoarrays. *Ultrasonics Sonochemistry*. 2009; 16:11-14. http://dx.doi.org/10.1016/j.ultsonch.2008.05.011
4. Wahab R, Ansari SG, Kim YS, Seo HK and Shin HS. Room temperature synthesis of needle-shaped ZnO nanorods via sonochemical method. *Applied Surface Science*. 2007; 253:7622-7626. http://dx.doi.org/10.1016/j.apsusc.2007.03.060
5. Pholnak C, Sirisathitkul C, Danworaphong S and Harding DJ. Sono-synthesized sword-like zinc oxide and its use as a filler in polyurethane composites. *Journal of Optoelectronics and Advanced Materials*. 2012; 14:441-447.
6. Pholnak C, Sirisathitkul C and Harding DJ. Characterizations of octahedral zinc oxide synthesized by sonochemical method. *Journal of Physics and Chemistry of Solids*. 2011; 72:817-823. http://dx.doi.org/10.1016/j.jpcs.2011.04.005
7. Xiao Q, Huang S, Zhang J, Xiao C and Tan X. Sonochemical synthesis of ZnO nanosheet. *Journal of Alloys and Compounds*. 2008; 459:L18-L22. http://dx.doi.org/10.1016/j.jallcom.2007.05.026
8. Pholnak C, Sirisathitkul C, Harding DJ and Suwanboon S. Sonochemical synthesis of ZnO nanotubes and their optical emissions. *Journal of the Ceramic Society of Japan*. 2011; 119:535-537. http://dx.doi.org/10.2109/jcersj2.119.535

9. Uma K, Ananthakumar S, Mangalaraja RV, Mahesh KPO, Soga T and Jimbo T. A facile approach to hexagonal ZnO nanorod assembly. *Journal of Sol-Gel Science and Technology*. 2009; 49:1-5. http://dx.doi.org/10.1007/s10971-008-1846-5
10. Lee BW, Kim TS, Goswami SK and Oh E. Gas sensitivity and point defects in sonochemically grown ZnO nanowires. *Journal of the Korean Physical Society*. 2012; 60:415-419. http://dx.doi.org/10.3938/jkps.60.415
11. Choi SC, Yun WS, Sohn SH and Oh SJ. Effects of the aspect ratio on the dye adsorption of ZnO nanorods grown by using a sonochemical method for dye-sensitized solar cells. *Journal of the Korean Physical Society*. 2012; 61:1444-1448. http://dx.doi.org/10.3938/jkps.61.1444
12. Gusatti M, Barroso GS, de Campos CEM, De Souza DAR, Do Rosário JD, Lima RB et al. Effect of different precursors in the chemical synthesis of ZnO nanocrystals. *Materials Research*. 2011; 14: 264-267. http://dx.doi.org/10.1590/S1516-14392011005000035
13. Hales MC and Frost RL. Synthesis and vibrational spectroscopic characterization of synthetic hydrozincite and smithsonite. *Polyhedron*. 2007; 26:4955-4962. http://dx.doi.org/10.1016/j.poly.2007.07.002
14. Wypych F, Arizaga GGC and Da Costa Gardolinski JEF. Intercalation and functionalization of zinc hydroxide nitrate with mono- and dicarboxylic acids. *Journal of Colloid and Interface Science*. 2005; 283:130-138. http://dx.doi.org/10.1016/j.jcis.2004.08.125
15. Haase M, Weller H and Henglein A. Photochemistry and radiation chemistry of colloidal semiconductors. *Journal of Physical Chemistry B*. 1988; 92:482-487. http://dx.doi.org/10.1021/j100313a047
16. Wu LL and Wu YS. Synthesis and optical characteristic of ZnO nanorod. *Journal of Materials Science*. 2007; 42:406-408. http://dx.doi.org/10.1007/s10853-006-0727-y
17. Long TF, Yin S, Takabatake K, Zhang P and Sato T. Synthesis and characterization of ZnO nanorods and nanodisks from zinc chloride aqueous solution. *Nanoscale Research Letters*. 2009; 4:247-253. http://dx.doi.org/10.1007/s11671-008-9233-2
18. Wu HB, Chan MN and Chan CK. FTIR characterization of polymorphic transformation of ammonium nitrate. *Aerosol Science and Technology*. 2007; 41:581-588. http://dx.doi.org/10.1080/02786820701272038
19. Wahab R, Ansari SG, Kim YS, Dar MA and Shin HS. Synthesis and characterization of hydrozincite and its conversion into zinc oxide nanoparticles. *Journal of Alloys and Compounds*. 2008; 461: 66-71. http://dx.doi.org/10.1016/j.jallcom.2007.07.029
20. Ghose S. The crystal structure of hydrozincite, $Zn_5(OH)_6(CO_3)_2$. *Acta Crystallographica*. 1964; 17:1051-1057.20.
21. Parvin T, Keerthiraj N, Ibrahim IA, Phanichphant S and Byrappa K. Photocatalytic degradation of municipal wastewater and brilliant blue dye using hydrothermal synthesized surface-modified silver-doped ZnO designer particles. *International Journal of Photoenergy*. 2010; 670610.
22. Bitenc M, Marinšek M and Orel ZC. Preparation and characterization of zinc hydroxide carbonate and porous zinc oxide particles. *Journal of the European Ceramic Society*. 2008; 28:2915-2921. http://dx.doi.org/10.1016/j.jeurceramsoc.2008.05.003
23. Zhu ZQ and Zhou J. Rapid growth of ZnO hexagonal tubes by direct microwave heating. *International Journal of Minerals, Metallurgy and Materials*. 2010; 17:80-85. http://dx.doi.org/10.1007/s12613-010-0114-1
24. Cheng HM, Hsu HC, Chen SL, Wu WT, Kao CC, Lin LJ et al. Efficient UV photoluminescence from monodispersed secondary ZnO colloidal spheres synthesized by sol-gel method. *Journal of Crystal Growth*. 2005; 277:192-199. http://dx.doi.org/10.1016/j.jcrysgro.2004.12.133
25. Huang Z, Yan D, Yang M, Liao X, Kang Y, Yin G et al. Preparation and characterization of the biomineralized zinc oxide particles in spider silk peptides. *Journal of Colloid and Interface Science*. 2008; 325:356-362. http://dx.doi.org/10.1016/j.jcis.2008.05.040
26. Zhang J, Sun LD, Yin JL, Su HL, Liao CS and Yan CH. Control of ZnO morphology via a simple solution route. *Chemistry of Materials*. 2002; 14:4172-4177. http://dx.doi.org/10.1021/cm020077h
27. Yang J, Li X, Lang J, Yang L, Gao M, Liu X et al. Effects of mineralizing agent on the morphologies and photoluminescence properties of Eu^{3+}-doped ZnO nanomaterials. *Journal of Alloys and Compounds*. 2011; 509:10025-10031. http://dx.doi.org/10.1016/j.jallcom.2011.08.021